Soils and Foundations 2015;55(3):559–574

HOSTED BY

The Japanese Geotechnical Society

Soils and Foundations

www.sciencedirect.com
journal homepage: www.elsevier.com/locate/sandf

A stress–strain description of saturated sand under undrained cyclic torsional shear loading

Laddu Indika Nalin De Silva[a,b,*], Junichi Koseki[c], Gabriele Chiaro[c], Takeshi Sato[d]

[a]Department of Civil Engineering, University of Moratuwa, Sri Lanka
[b]Department of Civil Engineering, University of Tokyo, Japan
[c]Institute of Industrial Science, University of Tokyo, Japan
[d]Integrated Geotechnology Institute Ltd., Japan

Received 21 January 2014; received in revised form 11 December 2014; accepted 2 February 2015
Available online 16 May 2015

Abstract

A constitutive model to describe the cyclic undrained behavior of saturated sand is presented. The increments in volumetric strain during undrained loading, which are equal to zero, are assumed to consist of increments due to dilatancy and increments due to consolidation/swelling. This assumption enables the proposed model to evaluate increments in volumetric strain due to dilatancy as mirror images of increments in volumetric strain due to consolidation/swelling, thus simulating the generation of excess pore water pressure (i.e., reduction in mean effective principal stress) during undrained cyclic shear loading. Based on the results of drained tests, the increments in volumetric strain due to consolidation/swelling are evaluated by assuming that the quasi-elastic bulk modulus can be expressed as a unique function of the mean effective principal stress. On the other hand, in evaluating the increments in volumetric strain due to dilatancy, a normalized stress–plastic shear strain relationship is employed in combination with a novel empirical stress–dilatancy relationship derived for torsional shear loading. The proposed stress–dilatancy relationship accounts for the effects of over-consolidation during cyclic loading. Numerical simulations show that the proposed model can satisfactorily simulate the generation of excess pore water pressure and the stress–strain relationship of saturated Toyoura sand specimens subjected to undrained cyclic torsional shear loading. It is found that the liquefaction resistance of loose Toyoura sand specimens can be accurately predicted by the model, while the liquefaction resistance of dense Toyoura sand specimens may be slightly underestimated. (i.e., the liquefaction potential is higher). Yet, the model predictions are conservative.

Keywords: Liquefaction behavior; Stress–dilatancy relationship; Over-consolidation; Sand; Constitutive model

JEL classification: IGC; A10; D07; E08; T06

1. Introduction

Earlier experimental attempts to study the liquefaction behavior of soils date back to the 1960s when Seed and Lee (1966) conducted a series of undrained cyclic triaxial tests on saturated sand and reported that the onset of liquefaction was primarily governed by the relative density of the sand, the confining pressure, the stress or strain amplitude and the

*Corresponding author.
E-mail addresses: nalinds@uom.lk (L.I.N. De Silva), koseki@iis.u-tokyo.ac.jp (J. Koseki), chiaroga@iis.u-tokyo.ac.jp (G. Chiaro), tsato@iis.u-tokyo.ac.jp (T. Sato).
Peer review under responsibility of The Japanese Geotechnical Society.

http://dx.doi.org/10.1016/j.sandf.2015.04.008

Nomenclature

$\tau_{z\theta}$	shear stress
$\sigma_z^{'}$, $\sigma_r^{'}$ and $\sigma_\theta^{'}$	axial, radial and circumferential effective stress, respectively
p'	mean effective stress
Dr_{ini}	relative density measured at confining pressure of 30 kPa
$(\tau_{z\theta}/p')_{max}$	maximum shear stress ratio
$\tau_{z\theta\ max}$	peak shear stress
$G_{z\theta 0}$	initial quasi-elastic shear modulus ($=d\tau_{z\theta}/d\gamma_{z\theta}^{e}$)
$\gamma_{z\theta}$, $\gamma_{z\theta}^{e}$, $\gamma_{z\theta}^{p}$	total, elastic and plastic shear strain, respectively (engineering strain)
ε_{vol}^{p}	plastic volumetric strain
γ_{ref}	reference shear strain ($=(\tau_{z\theta}/p')/(G_{z\theta 0}/p')$)
m, n, k	material parameters that accounts for the stress induced anisotropy of Young's moduli, shear moduli and Poisson's ratio, respectively
C_E, C_G	factors that account for the degradation of quasi-elastic Young's and shear moduli, respectively (assumed as zero in the present study)
A	$E_{z0}/E_{\theta 0}$, i.e. ratio of vertical to circumferential quasi elastic Young's moduli at isotropic stress state
Y	normalized shear stress ($=(\tau_{z\theta}/p')/(\tau_{z\theta}/p')_{max}$)
X	normalized shear strain ($=\gamma_{z\theta}^{p}/\gamma_{ref}$)
D_1 and D_2	drag parameters
D	plastic shear moduli immediately after reversal of stress/initial plastic shear moduli (i.e., damage parameter)
D_{ult}	minimum value for D
S	amount of hardening
S_{ult}	maximum value for S
OC	over-consolidation ratio
$-d\varepsilon_{vol}^{p}/d\gamma_{z\theta}^{p}$	dilatancy ratio
R_k	gradient of the empirical stress–dilatancy relationship
R_m	the maximum value for R_k
C	intercept of the empirical stress–dilatancy relationship
C_{min}	minimum value for C

number of loading cycles. Since then, extensive studies have been conducted on soil liquefaction throughout the world (Vaid and Thomas, 1995, among others) and a number of attempts have been made to define proper constitutive models to describe it (Liou et al., 1977; Liyanapathirana and Poulos, 2002, among others).

Based on the results of several series of experiments on saturated hollow cylindrical sand specimens, Towhata and Ishihara (1985a) proposed a unique correlation between the shear work and the generation of pore water pressure (PWP). Furthermore, the effects of the rotation of the principal stress axes on sand liquefaction were investigated by Towhata and Ishihara (1985b) using hollow cylindrical specimens subjected to cyclic torsional shear loading. However, compared to the large amount of experimental data existing on liquefaction and the undrained behavior of soils, very few models are available to successfully simulate the soil performance under cyclic undrained loading. Ishihara et al. (1975) proposed a model based on five postulates to trace the generation of the excess PWP of sand subjected to undrained irregular cyclic loading. This model qualitatively simulates the stress–strain relationships and the shear stress versus mean effective stress relationships.

A constitutive model to simulate the cyclic undrained behavior of sand, based on the multi-spring concept, was developed by Iai et al. (1992). In this model, commonly known as the "Towhata–Iai model", shear deformation is modeled by employing the multi-spring concept, and the generation of excess PWP is modeled using a unique correlation between the increments in excess PWP and shear work, as proposed by Towhata and Ishihara (1985a). Nishimura (2002) and Nishimura and Towhata (2004) modified the above model by expanding the multi-spring concept from two dimensions to three dimensions, while using an empirical stress–dilatancy relationship to model the generation of excess PWP by correlating the stress–dilatancy relationship to consolidation. Nevertheless, these models do not consider the inherent anisotropy of soils. Furthermore, the steady state during liquefaction and the continuous increase in shear strain with cyclic loading cannot be properly simulated.

An elasto-plastic constitutive model for sand, based on the non-linear kinematic hardening rule, was employed to investigate the effectiveness of the cement-mixing column method and the gravel drain method as countermeasures against liquefaction by means of a two-dimensional liquefaction analysis (Oka et al., 1992). Later, Oka et al. (1999) further modified this model by introducing a stress–dilatancy relationship that accounts for the damage to plastic stiffness at large levels of shear strain. In addition, several other constitutive models, based on the critical state framework, are proposed in the literature. Jefferies (1993) proposed a strain-hardening model, which utilizes the state parameter, to explain the behavior of very loose to very dense sand. A unified generalized plasticity model, based on the non-linear critical state line, was proposed by Ling and Yang (2006).

It should be noted that all the above-described models are based on either the critical state soil mechanics approach (e.g., Oka et al., 1992) or the energetic approach (Iai et al., 1992; Nishimura, 2002). In the current study a different and original approach is attempted by extending empirical relationships that are found to be reasonably consistent with the experimental observations. The undrained cyclic behavior of sand is simulated based on the response whereby the same sand is shown during drained cyclic loading. In fact, after appropriate normalization, the stress–strain relationship is found to be unique for drained and undrained conditions. Moreover, the generation of PWP during undrained loading can be described based on the volumetric strain response of sand during drained loading. This is done by improving the model proposed by De Silva and Koseki (2012) that can

accurately simulate the drained cyclic behavior of sand, i.e., the stress–strain relationship and the volumetric strain response.

However, no attempt has been made so far to utilize the above-mentioned approach in simulating the cyclic undrained behavior (i.e., liquefaction) of soil. The attempt is made in this paper, where a cyclic constitutive model is presented to describe the undrained cyclic behavior of sand. In the model, a simulation of the plastic volumetric strain due to dilatancy ($d\varepsilon^d_{vol}$) is combined with the consolidation/swelling behavior of sand to simulate the generation of excess PWP (i.e., a reduction in mean effective principal stress) and stress–shear strain relationships.

2. Test material and procedures

In order to support the modeling work, a series of drained and undrained cyclic torsional shear loading tests were conducted on saturated Toyoura sand specimens ($D_{50}=0.162$ mm, $e_{max}=0.966$, $e_{min}=0.600$, coefficient of uniformity $U_c=1.46$). Hollow cylindrical specimens, having dimensions of 20 cm in outer diameter, 12 cm in inner diameter and 30 cm in height, were prepared at initial relative densities (Dr_{ini}) of 21%, 56% and 75%, as measured at a confining pressure of 30 kPa. A modified air pluviation technique, in which the sand pluviation was completed in a radial direction while slowly moving the nozzle of the pluviator in alternate clockwise/anticlockwise directions, was employed in the current study to minimize the degree of anisotropy of the horizontal bedding plane of the hollow cylindrical specimens (see details in De Silva et al. (2006)).

A high-capacity medium-sized hollow cylinder apparatus, developed at the Institute of Industrial Science, University of Tokyo, was used for the testing program. A recently developed local deformation measurement technique was employed in the evaluation of quasi-elastic deformation properties and volumetric strain during isotropic loading for drained specimens in the current study. Refer to De Silva et al. (2005) for details on the torsional shear apparatus and local deformation measurement system used. In order to investigate the stress–dilatancy relationship of Toyoura sand, a series of drained cyclic torsional shear tests was conducted on loose and dense specimens, with $Dr_{ini}=56\%$ and 75%, respectively, while keeping the mean effective principal stress (p') constant at 100 kPa. Details of the stress paths employed in the drained cyclic tests are presented in De Silva and Koseki (2012). In addition to the above, a series of constant stress amplitude undrained cyclic torsional shear tests was conducted on Toyoura sand specimens, while keeping the specimen height constant, for a comparison with the model predictions. The stress paths of the cyclic undrained tests are shown in Table 1.

3. Framework for modeling of liquefaction behavior

Changes in p' during undrained loading cause the consolidation/swelling of a specimen, while changes in shear stress (τ) cause dilation. Therefore, the increments in volumetric strain ($d\varepsilon_{vol}$) during undrained loading, which are equal to zero, are assumed to consist of volumetric strain components due to both dilatancy ($d\varepsilon^d_{vol}$) and consolidation/swelling ($d\varepsilon^c_{vol}$), as expressed in Eq. (1).

$$d\varepsilon_{vol}=d\varepsilon^c_{vol}+d\varepsilon^d_{vol}=0. \quad (1)$$

Table 1
Stress paths and test conditions of liquefaction tests.

Test	Dr (%)	Stress paths
SAT 38	75.7	(1) IC ($\sigma_z'=\sigma_r'=\sigma_\theta'=50\rightarrow100$ kPa) (2) UTS ($\tau_{z\theta}=0\rightarrow22\rightarrow-22\rightarrow0$ kPa, until liquefaction at $p_0'=100$ kPa)
SAT 28	74.6	(1) IC ($\sigma_z'=\sigma_r'=\sigma_\theta'=50\rightarrow100$ kPa) (2) UTS ($\tau_{z\theta}=0\rightarrow30\rightarrow-30\rightarrow0$ kPa, until liquefaction at $p_0'=100$ kPa)
SAT 31	79.4	(1) IC ($\sigma_z'=\sigma_r'=\sigma_\theta'=50\rightarrow100$ kPa) (2) UTS ($\tau_{z\theta}=0\rightarrow40\rightarrow-40\rightarrow0$ kPa, until liquefaction at $p_0'=100$ kPa)
SAT 32	75.2	(1) IC ($\sigma_z'=\sigma_r'=\sigma_\theta'=50\rightarrow100$ kPa) (2) UTS ($\tau_{z\theta}=0\rightarrow60\rightarrow-60\rightarrow0$ kPa, until liquefaction at $p_0'=100$ kPa)
SAT 34	50.3	(1) IC ($\sigma_z'=\sigma_r'=\sigma_\theta'=50\rightarrow100$ kPa) (2) UTS ($\tau_{z\theta}=0\rightarrow30\rightarrow-30\rightarrow0$ kPa, until liquefaction at $p_0'=100$ kPa)
SAT 33	21.3	(1) IC ($\sigma_z'=\sigma_r'=\sigma_\theta'=50\rightarrow100$ kPa) (2) UTS ($\tau_{z\theta}=0\rightarrow30$ kPa, flow failure at $p_0'=100$ kPa)

Dr: relative density (%) measured at an isotropic stress state of $\sigma_c'=30$ kPa, IC: isotropic consolidation. UTS: undrained cyclic torsional shear loading, p_0'=Initial mean effective stress at start of cyclic undrained loading.

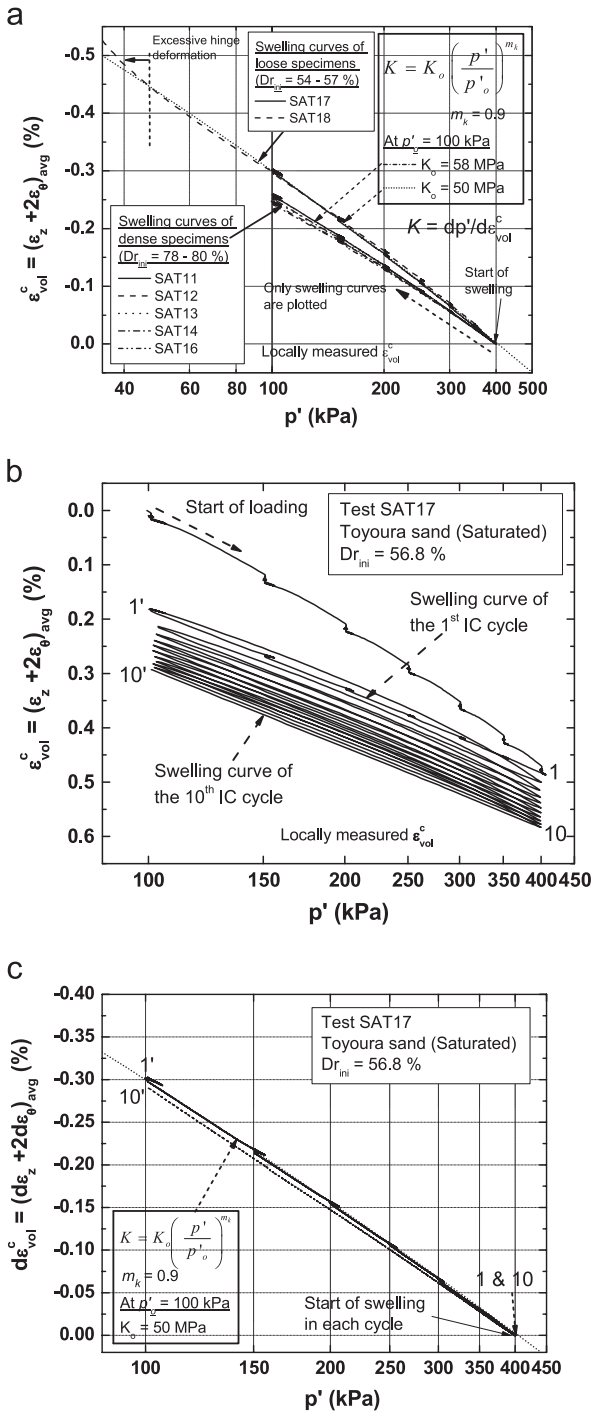

Fig. 1. Comparison of swelling curves for (a) loose and dense sand Toyoura sand specimens, (b) 10 isotropic cycles between $p'=100$ and 400 kPa of a typical loose specimen and (c) 1st and 10th cycles of a typical loose specimen.

4. Evaluation of $d\varepsilon^c_{vol}$

Fig. 1(a) shows volumetric strain (ε^c_{vol}) versus p' during the swelling of isotropically consolidated Toyoura sand specimens. It can be clearly seen that specimens of similar density have similar swelling curves. The ε^c_{vol} values reported in Fig. 1(a) are evaluated by employing the local deformation measurement (De Silva et al., 2005) and assuming the isotropy of the horizontal bedding plane (i.e., radial and circumferential strains, ε_r and ε_θ, respectively are equal). Local deformation measurement transducers (LDTs) are mounted on metal hinges, which are glued onto the membrane. However, excessive hinge deformation may take place when the confining stress becomes less than 50 kPa, causing an error when evaluating ε^c_{vol}, as shown in the upper left corner of Fig. 1(a).

In Fig. 1(a), it can also be observed that the swelling curves of Toyoura sand, subjected to isotropic unloading and reloading cycles in the range of p' from 100 to 400 kPa, can be expressed by Eq. (2).

$$d\varepsilon^c_{vol} = \frac{dp'}{K_o\left(\frac{p'}{p'_0}\right)^{m_k}} \tag{2}$$

where K_o is the bulk modulus at the reference mean effective stress (p'_0) and m_k is a material parameter. As shown in Fig. 1(a), it is found that the value for K_o (evaluated at $p'_0=100$ kPa) is 58 MPa for dense Toyoura sand specimens (Dr=75–80%) and 50 MPa for loose Toyoura sand specimens (Dr=54–57%). The value for m_k, for both dense and loose specimens, is taken as 0.9.

The effect of large isotropic loading/unloading cycles (IC cycles) on the swelling curve is shown in Fig. 1(b). Swelling curves for the first and tenth cycles are compared in Fig. 1(c). No significant effect on the swelling curve due to the application of isotropic cycles could be observed after applying 10 IC cycles (disregarding the effects of creep during the application of 10 cycles). Therefore, a unique swelling curve is employed in the current study to model ε^c_{vol}.

5. Modeling of monotonic stress–shear strain relationship

It is a well-known fact that $\tau_{z\theta}/p'$ versus plastic shear strain ($\gamma^p_{z\theta}$) during drained or undrained monotonic shear is of a non-linear shape (e.g., Koseki et al., 1998; among others). A typical relationship for a cyclic undrained test, conducted on a Toyoura sand specimen of $Dr_{ini}=75.7\%$, is shown in Fig. 2(a). $\gamma^p_{z\theta}$ is evaluated by deducting the elastic strain ($\gamma^e_{z\theta}$) components from the total shear strain ($\gamma_{z\theta}$). The $\gamma^e_{z\theta}$ component is evaluated by employing the quasi-elastic constitutive model (IIS model) proposed by HongNam and Koseki (2005, 2008). The parameters employed in the IIS model for a dense specimen with Dr_{ini} of about 75% (defined at a confining stress of 30 kPa) are listed in Table 2.

It should be mentioned that, when the soil reaches the full liquefaction state (i.e., $p'\approx 0$), the $\tau_{z\theta}/p'$ values become extremely sensitive to very small changes in p'. Hence, highly scattered data can be observed. Koseki et al. (2005) investigated the liquefaction properties of sand under low confining stress levels and proposed a simplified procedure to estimate the liquefaction resistance by introducing the concept of the apparent increase in effective mean principal stress ($\Delta p'$), due to particle interlocking, as well as parameter $\Delta\tau$ to correct τ due to possible measurement errors. Therefore, a modified stress ratio was proposed by Koseki et al. (2005): $(\tau_{z\theta}-\Delta\tau_{z\theta})/(p'+\Delta p')$. Chiaro et al. (2013) showed that the values for $\Delta\tau_{z\theta}$ and $\Delta p'$ may slightly vary during cyclic loading. However, for simplicity, the values for $\Delta\tau_{z\theta}$ and $\Delta p'$ were assumed to be constant, as originally suggested by Koseki et al.

(2005) in the present study. The modified stress ratio is employed in Fig. 2(a) with $\Delta\tau_{z\theta}=1.3$ kPa and $\Delta p'=0.2$ kPa. Typical evaluations of $\Delta\tau_{z\theta}$ and $\Delta p'$ are shown in Fig. 2(b). It can be clearly seen that $(\tau_{z\theta}-\Delta\tau_{z\theta})/(p'+\Delta p')$ versus $\gamma^p_{z\theta}$ is of a non-linear shape with hysteresis, which is similar to $\tau_{z\theta}/p'$ versus $\gamma^p_{z\theta}$ of a drained cyclic test.

In order to quantitatively investigate the above, comparisons of $\tau_{z\theta}/p'$ versus $\gamma^p_{z\theta}$ for the virgin loading of drained and undrained specimens of similar densities are shown in Fig. 3. It can be clearly seen that, for similar densities, $\tau_{z\theta}/p'$ versus $\gamma^p_{z\theta}$ for the undrained test is very similar to that for the drained test. This observation suggests that it is possible to evaluate $d\varepsilon^d_{\mathrm{vol}}$ (increment in volumetric strain due to dilatancy) during cyclic undrained loading by combining the simulation of the stress–shear strain relationship of a drained test with an appropriate stress–dilatancy relationship.

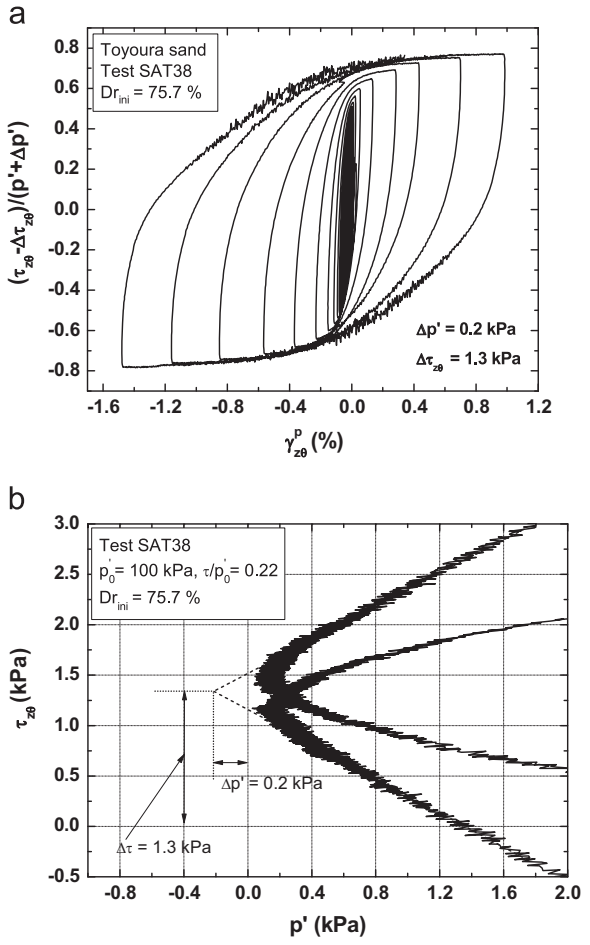

Fig. 2. (a) $(\tau_{z\theta}-\Delta\tau_{z\theta})/(p'+\Delta p')$ versus $\gamma^p_{z\theta}$ relationship of undrained test and (b) evaluation of $\Delta\tau_{z\theta}$ and $\Delta p'$.

Normalized stress–strain relationships during the virgin loading (backbone curves) of undrained tests with different densities are compared in Fig. 4. The peak shear stress ratio $((\tau_{z\theta}/p')_{\max})$ and the initial quasi-elastic shear modulus $(G_{z\theta 0})$ at $p'_0=100$ kPa for a specimen of $\mathrm{Dr_{ini}}=75\%$ were taken as 0.85 and 100 MPa, respectively, based on the results of a drained test on a specimen of similar density. For $\mathrm{Dr_{ini}}=50\%$, the $(\tau_{z\theta}/p')_{\max}$ and $G_{z\theta 0}$ values are 0.78 and 60 MPa, respectively, and for $\mathrm{Dr_{ini}}=21\%$, the $(\tau_{z\theta}/p')_{\max}$ and $G_{z\theta 0}$ values are 0.60 and 42.9 MPa, respectively. Reference shear strain γ_{ref} is taken as the ratio of $(\tau_{z\theta}/p')_{\max}$ to $G_{z\theta 0}/p'_0$.

Then, the Generalized Hyperbolic Equation (GHE), as proposed by Tatsuoka and Shibuya (1991) (Eq. (3)), was employed to simulate the backbone curve shown in Fig. 4.

$$Y=\frac{X}{\frac{1}{C_1(X)}+\frac{|X|}{C_2(X)}} \tag{3}$$

where

$$C_1(X)=\frac{C_1(0)+C_1(\infty)}{2}+\frac{C_1(0)-C_1(\infty)}{2}\cos\left(\frac{\pi}{\left(\frac{\alpha'}{X}\right)^{m_t}+1}\right) \tag{4a}$$

$$C_2(X)=\frac{C_2(0)+C_2(\infty)}{2}+\frac{C_2(0)-C_2(\infty)}{2}\cos\left(\frac{\pi}{\left(\frac{\beta'}{X}\right)^{n_t}+1}\right) \tag{4b}$$

and X and Y are normalized plastic shear strain and shear stress parameters, respectively. Normalized stress and strain parameters, as defined below, are selected by following the

Table 2
Model parameters.

Test	Quasi-elastic model parameters[a]	Drag parameters[b]	Hardening parameter[b], S_{ult}	Damage parameter[c], D_{ult}
SAT 38	$E_{zo}=215$ MPa, $\sigma'_o=100$ kPa, $\nu_{z\theta 0}=0.18$, $m=0.5$, $n=0.5$,	$D_1=0.15$	1.15	0.6
SAT 28	$k=0.3$, CE=CG=0.0, $a=0.7$			
SAT 31		$D_2=12$		
SAT 32				
SAT 34	$E_{zo}=190$ MPa, $\sigma'_o=100$ kPa, $\nu_{z\theta 0}=0.18$, $m=0.5$, $n=0.5$, $k=0.3$,	$D_1=0.01$		
	CE=CG=0.0, $a=0.7$	$D_2=3.13$		
SAT 33	$E_{zo}=145$ MPa, $\sigma'_o=100$ kPa, $\nu_{z\theta 0}=0.18$, $m=0.5$, $n=0.5$, $k=0.3$,	not required (specimen fails by flow failure)		
	CE=CG=0.0, $a=0.7$			

[a]Details of the formulation of the quasi-elastic model (IIS Model) and its parameters are presented in HongNam and Koseki (2005, 2008)

[b]Drag and hardening parameters are the same as those employed in the simulation of the stress–shear strain relationship during drained cyclic torsional shear loading in De Silva and Koseki (2012).

[c]Damage parameter D_{ult}, for drained cyclic loading, is taken as 0.2

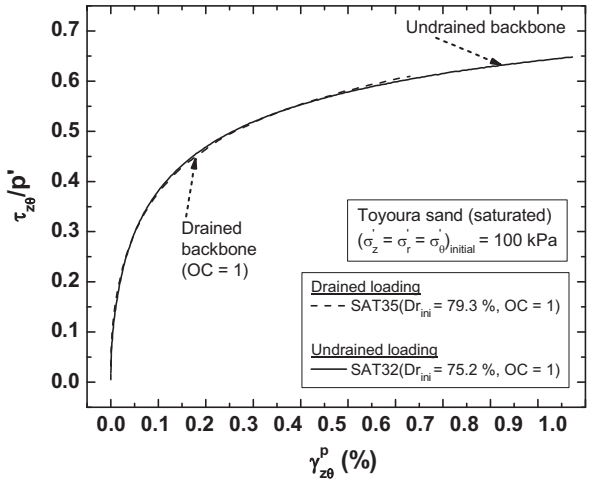

Fig. 3. Drained and undrained $\tau_{z\theta}/p'$ versus $\gamma^p_{z\theta}$ relationships during virgin loading.

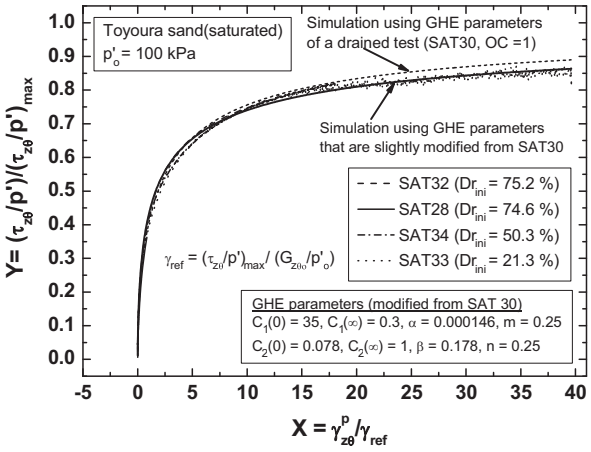

Fig. 4. Comparison of the backbone curves of undrained tests with different densities.

procedure proposed by De Silva and Koseki (2012):

$$X = \frac{\gamma^p_{z\theta}}{\gamma_{ref}} \quad \text{and} \quad Y = \frac{\tau_{z\theta}/p'}{(\tau_{z\theta}/p')_{max}} \tag{5}$$

where $\gamma^p_{z\theta} = \gamma_{z\theta} - \gamma^e_{z\theta}$ and $\gamma_{ref} = (\tau_{z\theta}/p')_{max}/(G_{z\theta 0}/p')$.

The GHE has 8 parameters, i.e., $C_1(0)$, $C_1(\infty)$, $C_2(0)$, $C_2(\infty)$, α', β', m_t and n_t, which can be determined from a single monotonic drained torsional shear test. Refer to Tatsuoka and Shibuya (1991) for the procedure for evaluating these parameters.

It can be seen from Fig. 4 that the normalized stress–shear strain relationships of undrained tests with different densities are similar. Hence, they can be modeled by employing a single set of GHE parameters obtained either by a normally consolidated drained test or an undrained shearing test. In order to obtain a better fitting to the experiment data, GHE parameters of undrained tests are selected by slightly modifying those of drained tests (Fig. 4).

6. Modeling of cyclic stress–shear strain relationship by using extended Masing's rule

Subsequent unloading/reloading cycles are modeled by employing the procedure proposed by De Silva and Koseki (2012), as briefed below.

Tatsuoka et al. (1997) reported that the stress–strain relationships of soils are significantly influenced by cyclic strain hardening, damage due to straining etc., which are caused by the rearrangement of particles during cyclic loading, and proposed additional rules to model these features to account for behaviors under more general stress conditions. In this regard, a conceptual approach was implemented for dense Toyoura sand under a plane strain condition by applying a horizontal shift to the basic skeleton curves, i.e., dragging the basic skeleton curve along the X-axis (strain parameter axis) in the opposite direction to its loading direction, while applying the (extended) Masing's rule (refer to Masuda et al. (1999) and Tatsuoka et al. (2003) for further details). It was assumed that the amount of drag β, applied to one basic skeleton curve in one loading direction, is a function of the plastic shear strain accumulated in the opposite loading direction (Masuda et al., 1999; Balakrishnaiyer and Koseki, 2000; Tatsuoka et al., 2003; HongNam and Koseki, 2008). The same approach was employed to model the cyclic stress–strain relationships of Toyoura sand under cyclic torsional shear loading (HongNam and Koseki, 2008; De Silva and Koseki, 2012). The dragged backbone curve can be written as follows:

$$Y = \frac{(X-\beta)}{\frac{1}{C_1(X-\beta)} + \frac{|X-\beta|}{C_2(X-\beta)}} \tag{6}$$

where β denotes the amount of drag, which can be evaluated by a drag function as shown below.

$$\beta = \frac{X'}{\frac{1}{D_1} + \frac{X'}{D_2}} \tag{7}$$

where D_1 is a fitting parameter (i.e., initial gradient of the drag function) and D_2 is the maximum amount of drag. D_1 and D_2 can be experimentally determined. X' is the accumulated normalized plastic shear strain in one direction (positive or negative direction).

HongNam and Koseki (2008) employed $D_1 = 0.45$ and $D_2 = 3.13$ for dense Toyoura sand ($Dr_{ini} = 71\%$) subjected to cyclic torsional shear loading starting from an isotropic stress state ($\sigma'_z = \sigma'_r = \sigma'_\theta = 100$ kPa). However, it was observed by De Silva and Koseki (2012) that the application of drag alone is not sufficient for simulating the cyclic stress–shear strain relationship close to the peak stress of the material.

6.1. Modification of extended Masing's rule

In view of the limitation of Masing's rule with drag in simulating the stress–shear strain relationship close to the peak stress of the material, De Silva and Koseki (2012) proposed two conceptual modification factors, which take into account the hardening behavior during cyclic loading (reduction in damping ratio with constant stress amplitude cyclic loading)

and damage to plastic stiffness ($d\tau_{z\theta}/d\gamma^p_{z\theta}$) at large stress levels, while maintaining continuity in the simulation.

The two parameters in the GHE, $C_1(X=0)$ and $C_2(X=\infty)$, represent the initial plastic stiffness and the peak strength, respectively. Therefore, the damage occurring to the plastic stiffness can be obtained by multiplying $C_1(X)$ by damage factor D, and the hardening can be obtained by multiplying $C_2(X)$ by hardening factor S. Note that in the approach used by Masuda et al. (1999), Balakrishnaiyer and Koseki (2000), and Tatsuoka et al. (2003), unique backbone curves were used to model subsequent cyclic branches by employing extended Masing's rules.

Therefore, the hysteresis curve, starting from an arbitrary point A, can be obtained by employing the extended Masing's rules with damage and hardening by using Eq. (8).

$$Y = Y_A + \frac{X - X_A}{\frac{1}{C_1\left(\frac{X-X_A}{n_p}\right)\times D} + \frac{|X-X_A|}{n_p \times C_2\left(\frac{X-X_A}{n_p}\right)\times S}} \tag{8}$$

In order to maintain continuity, the dragged backbone curve, which is in the same direction as the curve to be modeled, should be modified, as shown in Eq. (9), to determine the proportional parameter n_p by using the extended Masing's rules. Refer to Masuda et al. (1999) and Tatsuoka et al. (2003) for details on the extended Masing's rules and sub-rules.

$$Y = \frac{(X-\beta)}{\frac{1}{C_1(X-\beta)\times D} + \frac{|X-\beta|}{C_2(X-\beta)\times S}} \tag{9}$$

Note that parameters D and S were employed in Eqs. (8) and (9) in such a way that D and S are constant for a given hysteresis curve, but they change from curve to curve. An evaluation of D and S for a particular hysteresis curve is made based on a few empirical equations, as follows. The plastic shear modulus (D) can be expressed as an "S curve", as proposed by De Silva and Koseki (2012) and shown in Eq. (10).

$$D = D_{ult} + \frac{1+\exp(-\gamma^*)}{1+\exp\left(\left|\Delta\gamma^p_{z\theta}\right|_p - \gamma^*\right)}(1-D_{ult}) \tag{10}$$

where $|\Delta\gamma^p_{z\theta}|_p$ is the total plastic shear strain (%) accumulated between the current and the previous turning points, and D_{ult} is the minimum value for D, which would be applied to evaluate the minimum value for the plastic shear modulus. γ^* corresponds to the value for $\gamma^p_{z\theta}$ (in %) at which the volumetric behavior of the material changes from contractive to dilative, and is taken as 0.8.

De Silva and Koseki (2012) proposed $D_{ult}=0.2$ for drained cyclic torsional shear loading, although experimental evidence suggests that D_{ult} may lie between 0.2 and 0.6. In the current study, for an improved simulation of the experimental results, $D_{ult}=0.6$ is used for the case of cyclic undrained loading. Yet, it should be noted that the D value is assumed to be equal to 1.0 (i.e., no damage to the plastic shear modulus) until the volumetric behavior of the material changes from contractive to dilative at the phase transformation state (usually when $\tau_{z\theta}/p' \approx 0.5$ in the case of Toyoura sand).

In addition, De Silva and Koseki (2012) proposed a conceptual equation for hardening parameter S by assuming that S can be expressed as a hyperbolic function of the total normalized plastic strain up to the current turning point, as follows:

$$S = 1 + \frac{\left(\sum\left|\Delta X\right|\right)_{\text{Upto current turing point}}}{\frac{D_2}{D_1} + \frac{\left(\sum\left|\Delta X\right|\right)_{\text{Upto current turing point}}}{(S_{ult}-1)}} \tag{11}$$

where S_{ult} is the maximum value for S after applying an infinite number of cycles, and D_1 and D_2 are the same drag parameters used in Eq. (7). As suggested by De Silva and Koseki (2012), $S_{ult}=1.15$ was employed in the current study.

Note that the values for D_1 and D_2 differ for the cases with and without damage and hardening. HongNam and Koseki (2008) proposed $D_1=0.45$ and $D_2=3.13$ for Toyoura sand ($Dr_{ini}=71\%$) subjected to cyclic torsional shear loading starting from an isotropic stress state ($\sigma'_z=\sigma'_r=\sigma'_\theta=100$ kPa). After introducing the damage and hardening factors, $D_1=0.15$ and $D_2=12$ were found to be appropriate for dense Toyoura sand with $Dr_{ini}=75\%$, and $D_1=0.01$ and $D_2=3.13$ was suggested for Toyoura sand with $Dr_{ini}=50\%$ (De Silva and Koseki, 2012). The same values are employed for the respective densities in the simulation of undrained behavior. The concepts of drag, hardening and damage during drained cyclic torsional shear loading are illustrated in Fig. 5.

7. Evaluation of $d\varepsilon^d_{vol}$

In order to evaluate $d\varepsilon^d_{vol}$, it is necessary to combine $d\gamma^p_{z\theta}$ with an appropriate stress–dilatancy relationship. For the above purpose, the stress–dilatancy relationship, proposed by De Silva and Koseki (2012), is modified as follows.

During undrained cyclic loading, the mean effective stress (p') mainly decreases with the number of cycles. It is assumed in this study that the above reduction in p' is associated with

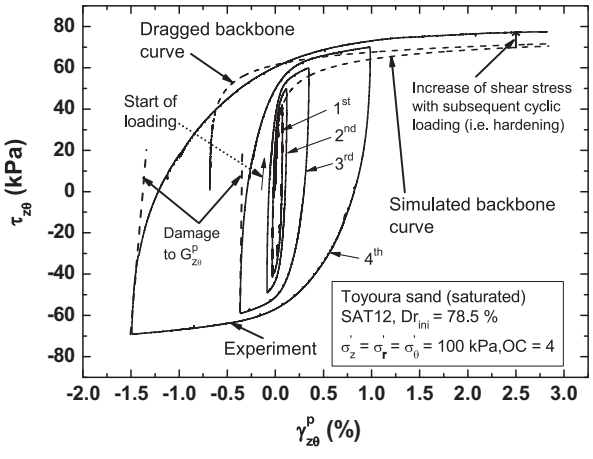

Fig. 5. Illustration of the concepts of drag, hardening and damage using a typical drained cyclic torsional shear test (De Silva and Koseki, 2012).

over-consolidation and cyclic mobility. Firstly, the soil undergoing a decrease in p' is subjected to over-consolidation until the stress state exceeds the phase transformation stress state (Ishihara and Li, 1972) for the first time (i.e., the first instance where the volumetric strain increment changes from contractive to dilative behavior, i.e., $d\varepsilon^d_{vol} < 0$). Then, the soil will enter the stage of cyclic mobility.

7.1. Stress–dilatancy relationship during virgin loading and before exceeding the phase transformation stress state

It can be observed in Fig. 6(a) and (b) that the stress–dilatancy relationship during cyclic loading before exceeding the phase transformation stress state is different from that after exceeding the phase transformation stress state (refer to the explanations given within Fig. 6(a) and (b)). In addition, it can be observed from Fig. 6(a) that the effects of over-consolidation significantly alter the stress–dilatancy relationship during virgin loading (refer to the line shown as "start of loading" in Fig. 6(a)). Since sand will be subjected to over-consolidation/swelling during undrained cyclic loading, the stress–dilatancy relationships during different stages are addressed separately in the current study.

The stress–dilatancy relationships, employed in the evaluation of $d\varepsilon^d_{vol}$, consist of four equations, namely, Eqs. (A), (B), (C) and (D) in Fig. 7(a). The stress–dilatancy model is summarized in Table 3. According to the proposed model, the stress–dilatancy relationship during the virgin loading of normally consolidated Toyoura sand is given by Eq. (12) (refer to Eq. (A) of Fig. 7(a)) with $R_k = 1.3$ and $C = 0.6$.

$$\frac{\tau_{z\theta}}{p'} = R_k\left(-\frac{d\varepsilon^d_{vol}}{d\gamma^p_{z\theta}}\right) \pm C \quad \text{for} \quad d\gamma^p_{z\theta} > 0 \quad \text{and} \quad d\gamma^p_{z\theta} < 0, \quad \text{respectively} \tag{12}$$

Since Toyoura sand was subjected to undrained cyclic torsional shear loading from a normally consolidated stress state, $d\varepsilon^d_{vol}$ during virgin loading was evaluated in the current study by applying the stress–dilatancy relationship for virgin loading, as given by Eq. (A) in Fig. 7(a).

If the loading direction after virgin loading is reversed before exceeding the phase transformation stress state, a different linear relationship is employed, by referring to Fig. 6, to account for the

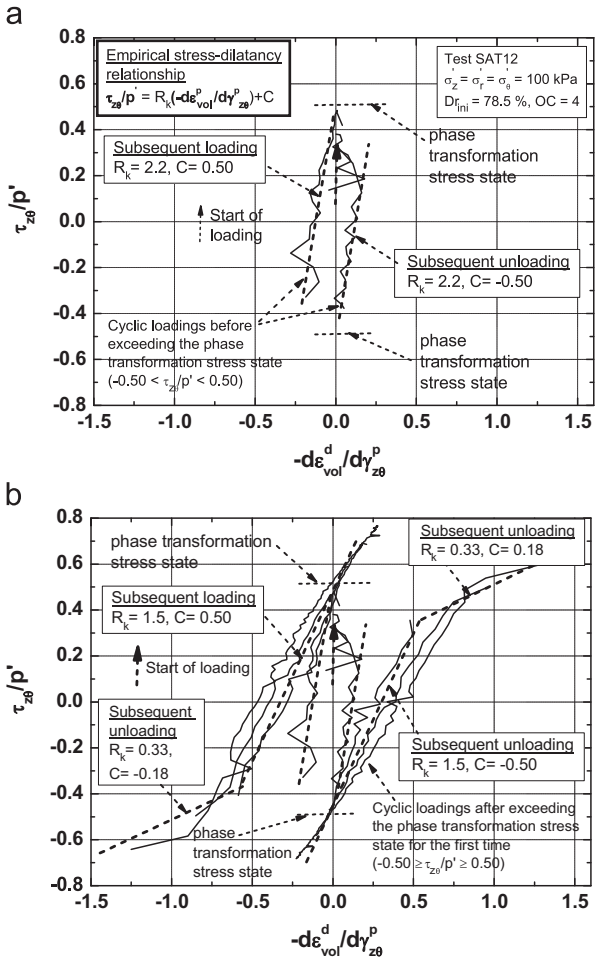

Fig. 6. Stress–dilatancy relationships during cyclic torsional shear loading (a) before exceeding the phase transformation stress state for the first time and (b) bilinear stress–dilatancy relationship after exceeding the phase transformation stress state.
Adopted from De Silva et al. (2014).

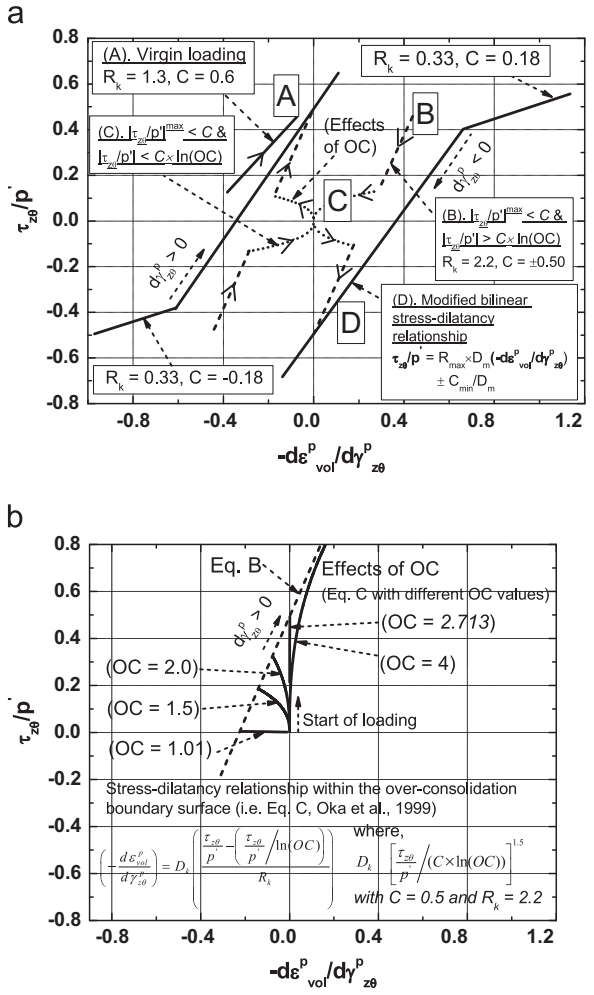

Fig. 7. Proposed stress–dilatancy relationships for (a) different stress states during undrained cyclic torsional shear loading of dense sand and (b) the stress state within the over-consolidation boundary surface.
Adopted from De Silva et al. (2014).

Table 3
Stress–dilatancy relationships to evaluate $d\varepsilon_{vol}^{d}$ during undrained cyclic loading.

Simulation case	Stress–dilatancy relationships		
	Virgin loading[a]	Subsequent loading	
Case 1 (Bilinear)	Eq. (A) with $R_k = 1.3,\ C = 0.6$	Eq. (A) with $R_k = 1.5, C = 0.5$ and Eq. (A) with $R_k = 0.33,\ C = 0.18$ for immediately after stress reversal	
Case 2 (Modified bilinear)	Eq. (A) with $R_k = 1.3,\ C = 0.6$	**If** $\left\|\tau_{z\theta}/p'\right\|^{max} \le \left\|C\right\|$ Eq. (B) with $R_k = 2.2, C = 0.5$for both dense ($Dr_{ini} \approx 75\%$) and loose ($Dr_{ini} \approx 50\%$) Toyoura sand, respectively **(Case 2.1)**	**If** $\left\|\tau_{z\theta}/p'\right\|^{max} > \left\|C\right\|$ Eq. (D) with $R_{max} = 1.5,\ C_{min} = 0.36$and Eq. (A) with $R_k = 0.33, C = 0.18$ for immediately after stress reversal
Case 3 (Modified bilinear+Effects of OC)	Eq. (A) with $R_k = 1.3,\ C = 0.6$	**If** $\left\|\tau_{z\theta}/p'\right\|^{max} \le \left\|C\right\|$ $\left\|\tau_{z\theta}/p'\right\| > \left\|C \times \ln(OC)\right\|$ Same as **Case 2.1** $\left\|\tau_{z\theta}/p'\right\| \le \left\|C \times \ln(OC)\right\|$ Eq. (C) with $R_k = 2.2,\ C = 0.5$ for both dense ($Dr_{ini} = 75\%$) and loose ($Dr_{ini} = 50\%$) specimens, respectively	Eq. (D) with $R_{max} = 1.5,\ C_{min} = 0.36$and Eq. (A) with $R_k = 0.33, C = 0.18$for immediately after stress reversal

OC: over-consolidation ratio.
[a]Virgin loading always starts from a normally consolidated stress state in the current study $\left\|\tau_{z\theta}/p'\right\|^{max}$: the maximum value of $\left\|\tau_{z\theta}/p'\right\|$ currently applied to the specimen.

hardening behavior until the stress state exceeds the phase transformation stress state for the first time (refer to steep dashed lines in Fig. 6(a) and (b)). Refer to the stress–dilatancy relationship denoted by Eq. (B) in Fig. 7(a) for further details. Eq. (B), as shown in Fig. 7(a), is obtained by employing $R_k = 2.2$ and $C = 0.5$ in Eq. (12) for both dense and loose Toyoura sand ($Dr_{ini} = 75\%$ or $Dr_{ini} = 50\%$).

7.2. Effects of over-consolidation on stress–dilatancy relationship

The over-consolidation ratio (OC) continuously changes (i.e., increases) when the cyclic loading continues within the limits of the phase transformation stress state (i.e., $|\tau_{z\theta}/p'| < C$). Hence, the effects of the change in OC on the stress–dilatancy relationship, within the above stress range, are taken into account by applying Eq. (13) (Oka et al., 1999) (refer to Eq. (C) in Fig. 7(a)). Note that the model by Oka et al. (1999) was formulated using the stress and strain invariants, while maintaining the objectivity. For simplicity, on the other hand, the stress–dilatancy relationship formulated in this study is described one-dimensionally using specific stress components. As will be described at the end of Section 9, an attempt is under way to extend the current stress–strain description into a generalized three-dimensional modeling.

For $d\tau_{z\theta} > 0$ and $d\tau_{z\theta} < 0$:

$$\left(-\frac{d\varepsilon_{vol}^{p}}{d\gamma_{z\theta}^{p}}\right) = D_k\left(\frac{\frac{\tau_{z\theta}}{p'} - \left(\frac{\tau_{z\theta}}{p'}/\ln(OC)\right)}{R_k}\right) \tag{13}$$

where $D_k = \left(\left|\frac{\tau_{z\theta}}{p'}/(C \times \ln(OC))\right|\right)^{1.5}$

The D_k value changes with OC. It is assumed that Eq. (13) continues until $D_k = 1$ with $R_k = 2.2$ and $C = 0.50$ for both dense and loose specimens and then follows Eq. (13) with $D_k = 1$ (i.e., changes in D_k due to changes in the stress state are not considered after $D_k > 1$). Refer to the stress–dilatancy relationship denoted by Eq. (C) in Fig. 7(a) for details. The stress state at which $D_k = 1$ is defined as the over-consolidation boundary surface (Oka et al., 1999).

When $D_k = 1$

$$C = \frac{\tau_{z\theta}}{p'}/\ln(OC) \tag{14}$$

Then, Eq. (13) can be rewritten as follows:

$$\left(-\frac{d\varepsilon_{vol}^{p}}{d\gamma_{z\theta}^{p}}\right) = \left(\frac{\frac{\tau_{z\theta}}{p'} - C}{R_k}\right) \tag{15}$$

Eq. (15) corresponds to Eq. (B) in Fig. 7(a). After that, the stress–dilatancy relationship follows Eq. (15) until the stress state exceeds the phase transformation stress state for the first time and then follows the modified bilinear stress–dilatancy relationship (Eq. (D) shown in Fig. 7(a)).

In short, if stress reversal occurs before exceeding the phase transformation stress state, the stress–dilatancy relationship follows a combination of Eqs. (B) and (C) until the stress state exceeds the phase transformation stress state for the first time. The combination of Eqs. (B) and (C), for $d\tau_{z\theta} > 0$ with different values for OC, is illustrated in Fig. 7(b).

Rearranging the terms in Eq. (14), we get the over-consolidation boundary surfaces for positive and negative shear stress increments, as shown in Eqs. (16a) and (16b).

For $d\tau_{z\theta} > 0$:

$$\tau_{z\theta} = C \times p' \times \ln(OC) \tag{16a}$$

Similarly, for $d\tau_{z\theta} < 0$:

$$\tau_{z\theta} = -C \times p' \times \ln(OC) \tag{16b}$$

Fig. 8 shows a typical over-consolidation boundary surface for a normally consolidated specimen subjected to cyclic undrained torsional shear loading starting from $p_0' = 100$ kPa.

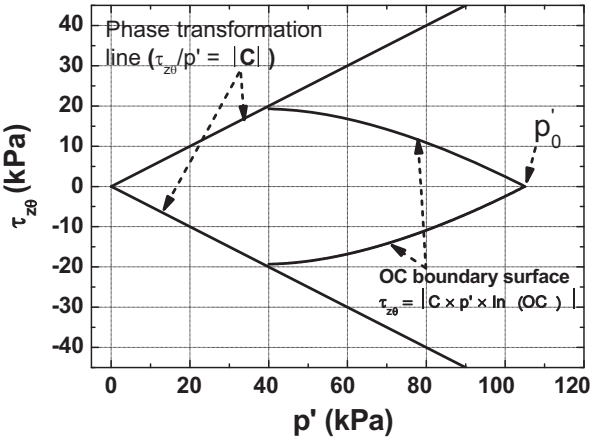

Fig. 8. Typical over-consolidation boundary surface and phase transformation stress state for a normally consolidated specimen with no initial shear.

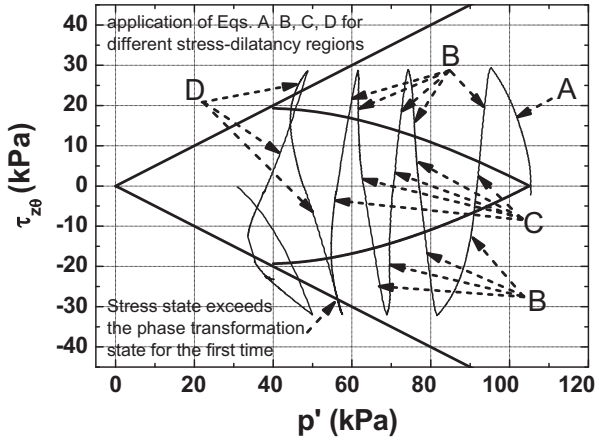

Fig. 9. Application of different stress–dilatancy relationships for different stress states during undrained cyclic torsional shear loading.

The phase transformation stress state for the above specimen is also indicated in Fig. 8.

7.3. Stress–dilatancy relationship after exceeding the phase transformation stress state

If the loading direction during virgin loading is reversed after exceeding the phase transformation stress state, the stress–dilatancy relationship will follow the modified bilinear stress–dilatancy relationship, as given below, for subsequent cyclic loadings (refer to Eq. (D) in Fig. 7(a)).

$$\frac{\tau_{z\theta}}{p'} = (R_{\max} \times D) \times \left(\frac{-d\varepsilon_{\mathrm{vol}}^{d}}{d\gamma_{z\theta}^{p}}\right) \pm \frac{C_{\min}}{D} \tag{17}$$

where $R_{\max}$ is the maximum value for R_k in Eq. (12) (i.e., $R_{\max}=1.5$ adopted from De Silva et al. (2014)), $C_{\min}$ is the minimum value for C after application of a large number of constant stress amplitude cyclic loadings (i.e., $C_{\min}=0.36$ adopted from De Silva et al. (2014)) and D is the same damage parameter as in Eq. (10).

The following boundary conditions were specified for the $R_{\max} \times D$ and $C_{\min}/D$ values by referring to the experimental data (based on De Silva et al. (2014)). Note that, $R_{\max} \times D$ should not be less than 1.0. The maximum value for $C_{\min}/D$ should not be larger than 0.60. Therefore, the $R_{\max} \times D$ value in Eq. (2) varies between 1.5 and 1.0, while the $C_{\min}/D$ value varies between 0.36 and 0.60 depending on the accumulated plastic strain between the current and the previous turning points (i.e., damage parameter D).

The application of different stress–dilatancy equations for different stress states during a typical cyclic undrained test is illustrated in Fig. 9. The four-phase stress–dilatancy model, employed in the current study, is summarized in Table 3.

By combining Eq. (1) with (2), the following equation can be derived to evaluate the change in mean effective stress (dp') during undrained cyclic loading:

$$dp' = K_o \left(\frac{p'}{p_o'}\right)^{m_k} (-d\varepsilon_{\mathrm{vol}}^{d}) \tag{18}$$

where $d\varepsilon_{\mathrm{vol}}^{d}$ is the volumetric strain increment due to dilatancy, which is evaluated by combining the simulation of stress–shear strain relationship during drained cyclic torsional loading with the proposed stress–dilatancy model. Then, by the numerical integration of Eq. (18), the generation of excess PWP with the shear stress level (or p' versus $\tau_{z\theta}$) can be established. In addition, the stress–strain relationship (i.e., $\tau_{z\theta}$ versus $\gamma_{z\theta}^{p}$) can also be obtained.

8. Simulation of liquefaction behavior

8.1. Dense sand behavior

The experimentally obtained effective stress path ($\tau_{z\theta}$ versus p') and stress–shear strain relationships ($\tau_{z\theta}$ versus $\gamma_{z\theta}$) of a dense Toyoura sand specimen, subjected to undrained cyclic torsional shear loading with stress amplitude ($\tau_{z\theta}/p_o'$) equal to 0.22, are shown in Fig. 10(a) and (a_1), respectively. In order to show the improvement in the simulation results with the introduction of the modifications to the stress–dilatancy relationship, a simulation of the stress paths was carried out in three steps, as denoted by (b), (c) and (d) in Fig. 10. The corresponding stress–strain relationships are denoted by (b_1), (c_1) and (d_1), respectively.

First, a unique bilinear stress–dilatancy relationship (refer to De Silva et al. (2014) for details), without considering any effects of over-consolidation or change in the stress–dilatancy relationship with cyclic loading, is employed (refer to Case 1 in Table 3). The simulated stress path and the stress–strain relationship that corresponds to each of the above stress–dilatancy relationships are shown in Fig. 10(b) and (b_1), respectively. It can be seen that the reduction in the change in p', due to the effects of over-consolidation (see Fig. 10(a)), cannot be accurately simulated by employing the above stress–dilatancy relationship, as shown in Fig. 10(b). In addition, dense Toyoura sand shows a continuous increase in shear strain after the onset of cyclic mobility, as shown in Fig. 10 (a_1), which is similar to that of a loose sand specimen, and ends up yielding the same curve (closed loop) for subsequent cycles, as shown in Fig. 10(b_1).

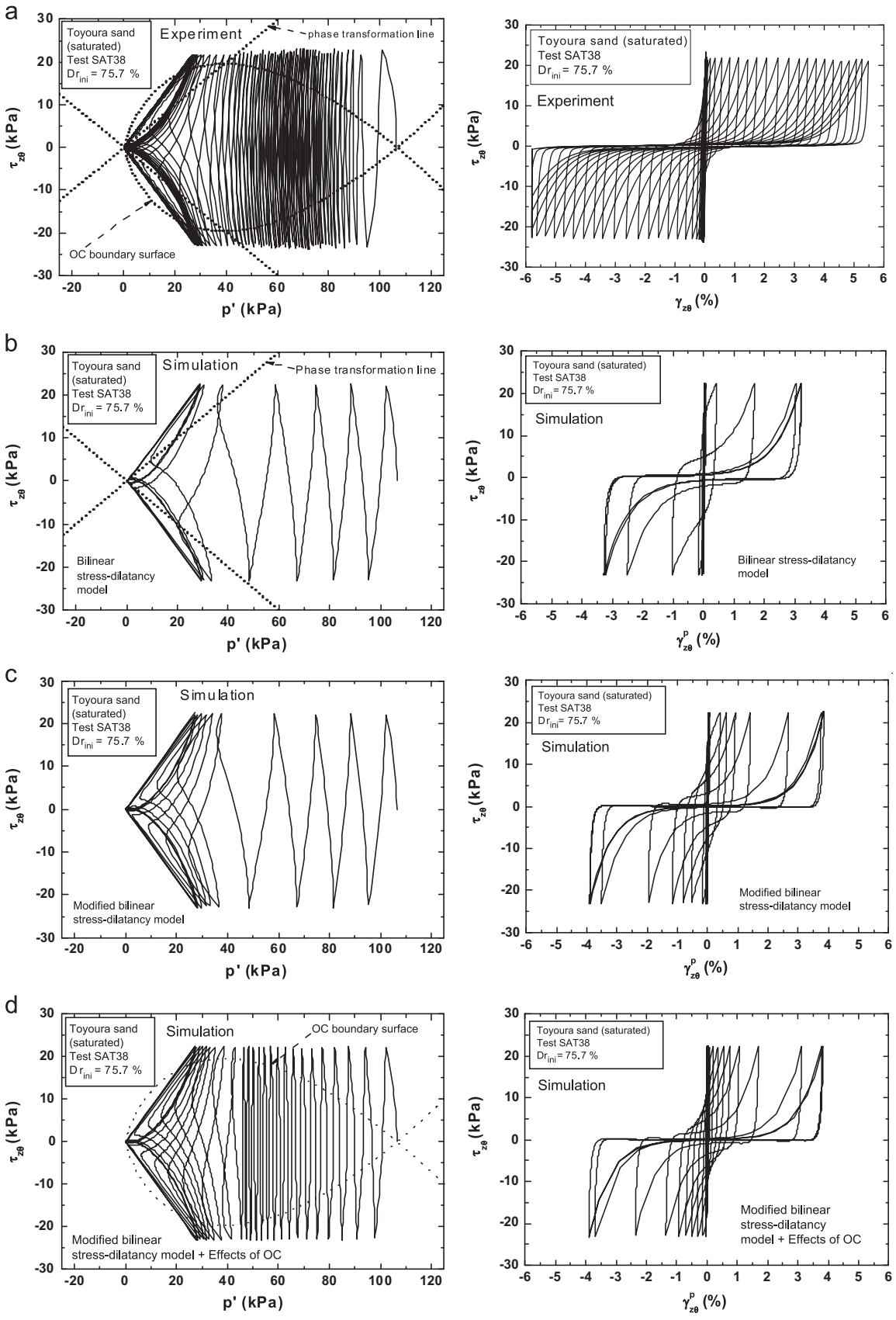

Fig. 10. Simulations of stress paths and stress–strain relationships using different stress–dilatancy relationships ($\tau_{z\theta}/p' = 0.22$, $Dr_{ini} = 75.7\%$).

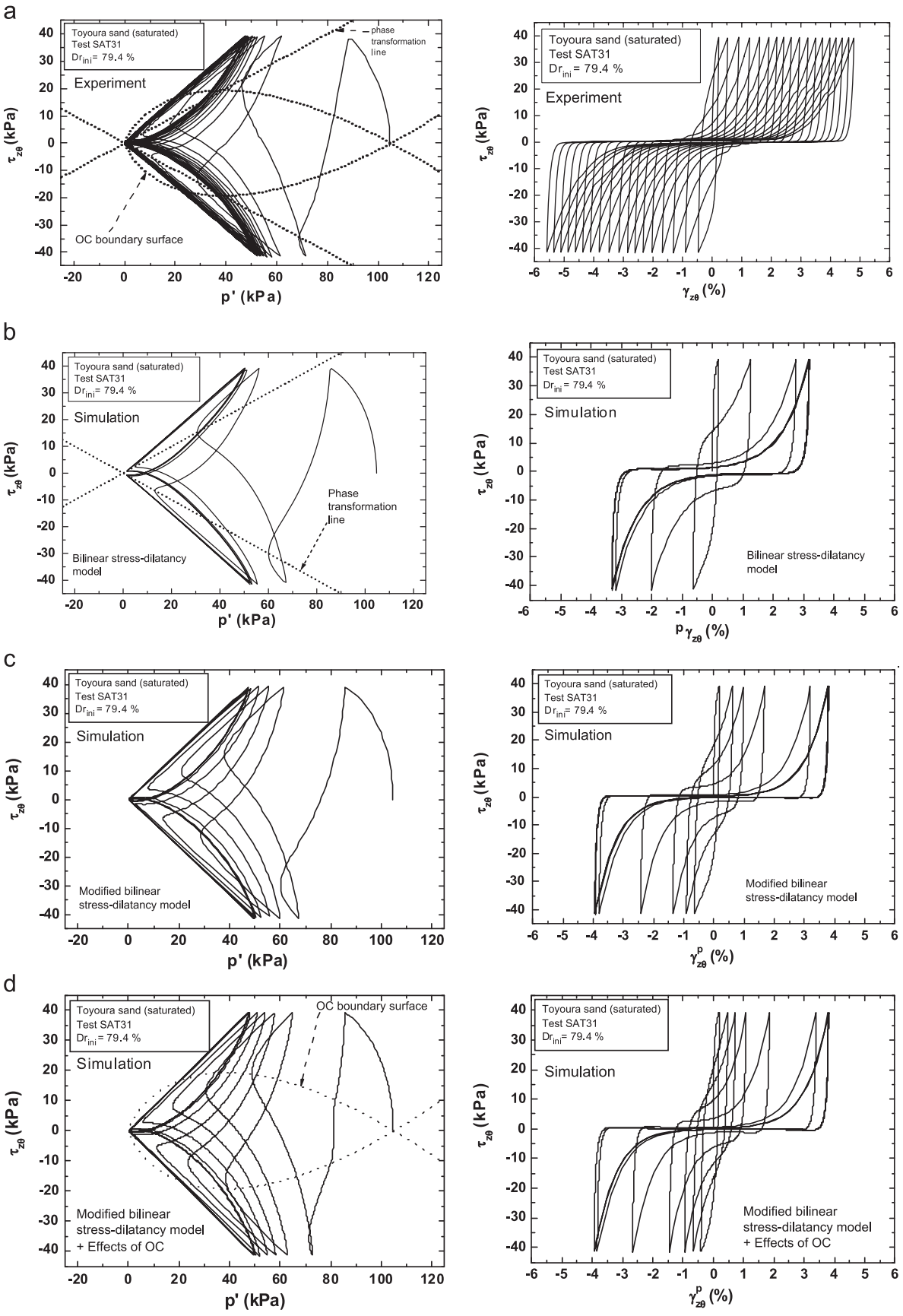

Fig. 11. Simulations of stress paths and stress–strain relationships using different stress–dilatancy relationships ($\tau_{z\theta}/p'=0.40$, $Dr_{ini}=79.4\%$).

Consequently, the variations in the stress–dilatancy relationship during cyclic loading are taken into account in the simulation by employing the modified bilinear stress–dilatancy relationship (refer to De Silva et al. (2014)) without considering any effects due to over-consolidation (refer to Case 2 in Table 3). It can be seen from Fig. 10(c) that the stress path after the onset of cyclic mobility is improved and, in addition, the stress–strain relationship is improved to some extent showing a continuous increase in shear strain with cyclic loading after the onset of cyclic mobility, as shown in Fig. 10 (c_1). However, when the stress path enters the steady state, the stress–strain relationship becomes a closed loop. Furthermore, since the effects of over-consolidation are not taken into account in the above simulation, the reduction in the change in p' due to the effects of over-consolidation, as shown in Fig. 10(a), cannot be accurately simulated.

Finally, the further modified stress–dilatancy model, summarized in Case 3 (Table 3), which considers the effects of over-consolidation and changes in the stress–dilatancy relationship during cyclic loading, was employed in the simulation of the stress path and stress–strain relationships during undrained cyclic loading, as shown in Fig. 10(d) and (d_1), respectively. It can be observed that the simulations for both the stress path and the stress–strain relationship are certainly

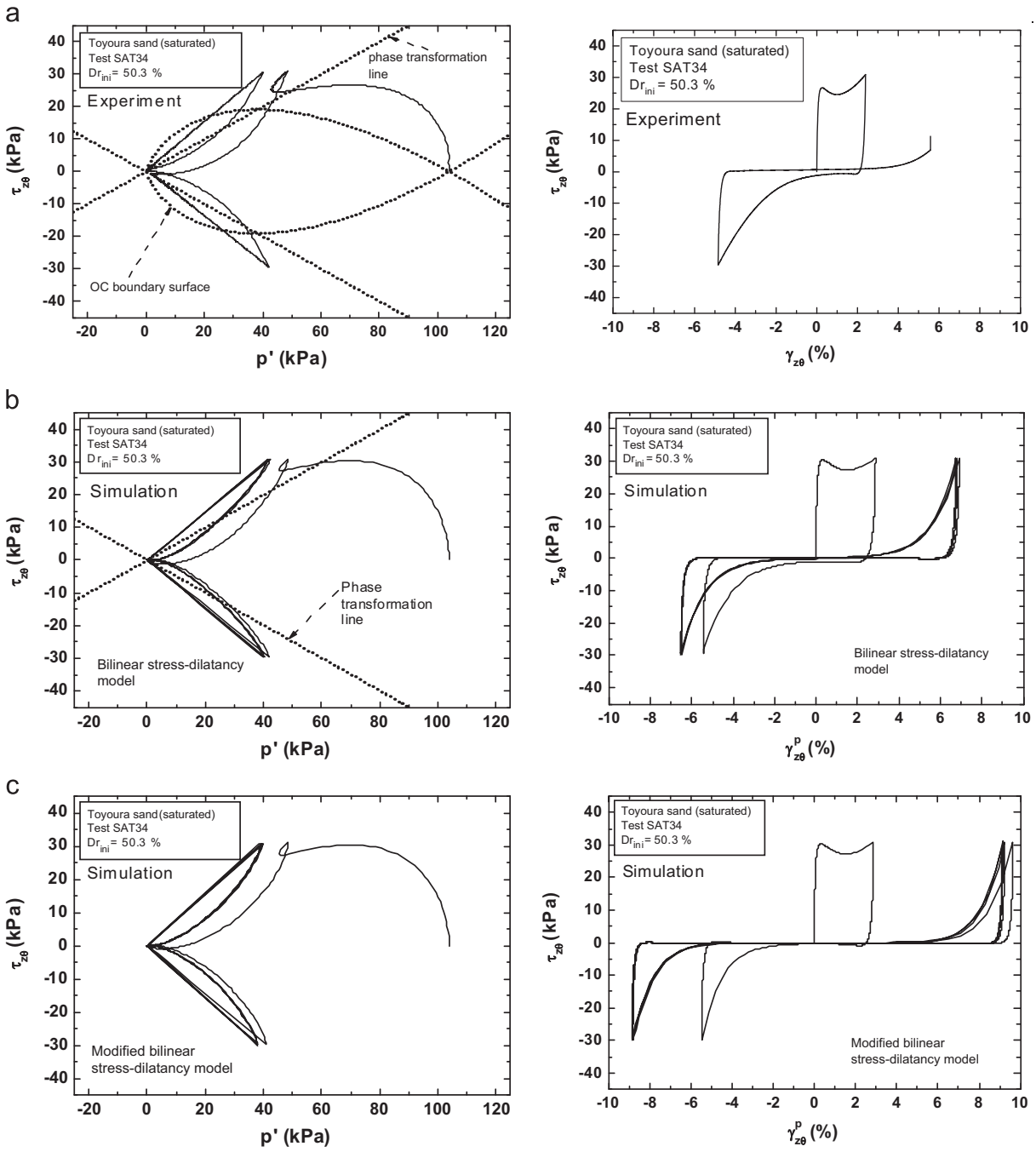

Fig. 12. Simulations of stress paths and stress–strain relationships using different stress–dilatancy relationships ($\tau_{z\theta}/p' = 0.30$, $Dr_{ini} = 50.3\%$).

improved after introducing the effects of over-consolidation into the modified bilinear stress–dilatancy relationship. A continuous increase in strain can be observed until the stress path enters the steady state.

It should be noted that the simulation started producing the same curve when $|\gamma^p_{z\theta}|$ was close to about 4%, while the experimental data shows a continuous increase in shear strain with cyclic loading. This strain level ($|\gamma^p_{z\theta}|=4\%$) is close to the strain level at which the peak stress state of dense Toyoura sand is mobilized in drained shearing. Further modification of the stress–strain relationship, which considers the strain-softening behavior observed during cyclic torsional shear loading (Kiyota et al., 2008), would be necessary to address the above issue for dense sand. However, this was not attempted in the current study. Since the simulation of the stress–strain relationship of dense Toyoura sand subjected to cyclic undrained loading using the bilinear stress–dilatancy model (refer to Fig. 10(b_1)) gives the same curve when $\left|\gamma^p_{z\theta}\right| \approx 3\%$, liquefaction resistance is defined in the current study as the number of cycles required to yield a double amplitude shear strain of 6%.

A comparison of the experimental stress paths and the stress–strain relationships of dense Toyoura sand specimens, subjected to undrained cyclic torsional shear loading, with their simulation results for stress amplitudes ($\tau_{z\theta}/p'_o$) equal to 0.40, is shown in Fig. 11. The same stress–dilatancy relationships as employed in Fig. 10(b)–(d) are utilized in Fig. 11.

8.2. Loose sand behavior

The experimental effective stress paths and stress–strain relationships of a loose Toyoura sand specimen ($Dr_{ini}=50\%$) with stress amplitudes ($\tau_{z\theta}/p'_o$) equal to 0.30 are shown in Fig. 12(a) and (a_1), respectively. It can be seen in Fig. 12(c) and (c_1) that the simulations of the stress path and the stress–strain relationship, respectively, become consistent with the corresponding experimental data when the modified bilinear stress–dilatancy relationship is employed (compare Fig. 12(a) and (a_1) with Fig. 12(c) and (c_1), respectively). The simulation continues until the double amplitude of shear strain becomes about 18% and then gives the same curve for further cycles.

Fig. 13(a) compares the experimentally obtained stress paths of a very loose specimen ($Dr_{ini}=21.3\%$) with its simulation, while Fig. 13(b) compares the experimentally and numerically obtained stress–strain relationships. Note that the specimen shows flow failure and the simulation shows a similar tendency. Therefore, only the stress–dilatancy relationship during virgin loading (refer to Table 3) is required for the simulation.

8.3. Liquefaction resistance curve

Fig. 14(a) and (b) shows the liquefaction resistance curves for dense and loose Toyoura sand specimens, respectively. In the current study, liquefaction resistance is defined as the number of cycles required to yield a double amplitude shear strain of 6%. In each figure, the liquefaction resistance curve

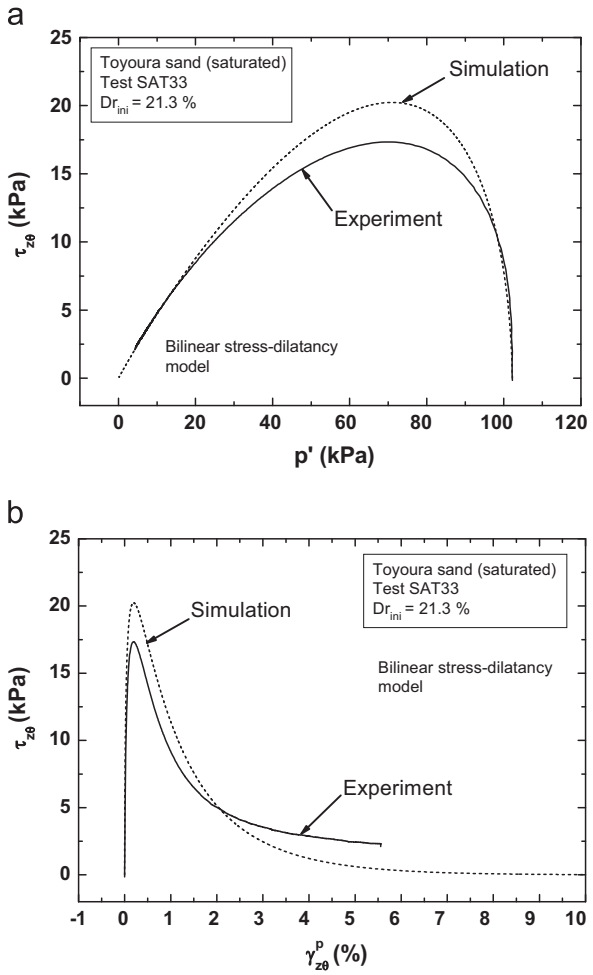

Fig. 13. Comparison of (a) stress paths and (b) stress–strain relationships ($Dr_{ini}=21.3\%$).

obtained from the experimental data is compared with that obtained from the simulation results by employing different stress–dilatancy relationships. However, it can be seen that the simulation was significantly improved when the modified bilinear stress–dilatancy relationship was employed while considering the effects of over-consolidation. It can be seen that the liquefaction resistance of dense Toyoura sand specimens is underestimated (i.e., in the simulation liquefaction occurs faster) by the simulated results. On the other hand, the experimentally evaluated liquefaction resistance curves of the loose Toyoura sand specimens (obtained using data from this study and Chiaro et al., 2012) are similar to those obtained from the simulation results after employing the modified bilinear stress–dilatancy relationship with the effects of over-consolidation (refer to Fig. 14(b)).

9. Conclusions

The following main conclusions can be derived from the above study:

(1) A unique swelling curve, that does not change with the number of cycles, has been proposed to evaluate the

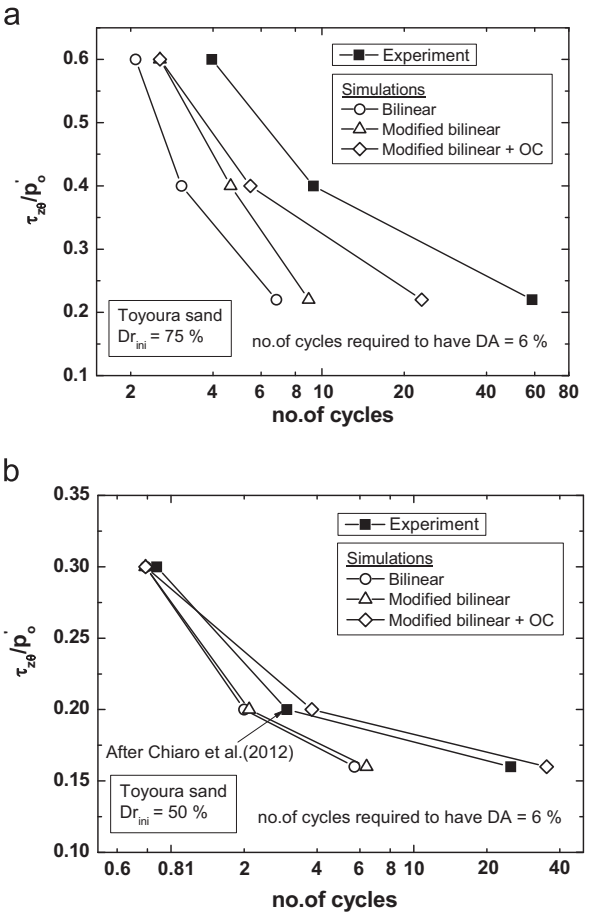

Fig. 14. Liquefaction resistance curves: (a) dense Toyoura sand, $Dr_{ini}=75\%$ and (b) Loose Toyoura sand, $Dr_{ini}=50\%$.

increments in volume change due to consolidation/swelling during undrained cyclic loading.

(2) The normalized stress–shear strain relationships of undrained tests with different densities were found to be similar. Hence, they can be modeled by employing a single set of GHE parameters obtained either by normally consolidated drained tests or undrained shearing tests.

(3) $\tau_{z\theta}/p'$ versus $\gamma^{p}_{z\theta}$ of an undrained specimen is very similar to that of a normally consolidated drained specimen of similar density. Hence, similar GHE parameters can be used for a drained normally consolidated specimen to evaluate the increments in volume change due to the dilatancy of an undrained specimen. In addition, drag parameters, damage parameters and hardening parameters were also similar for both drained and undrained loadings.

(4) The stress path during undrained cyclic loading is divided into four sections, namely (1) virgin loading, (2) stress path within the limits of phase transformation stress state, (3) stress path within the limits of over-consolidation boundary surfaces and (4) stress path after exceeding the phase transformation stress state for the first time. Different stress–dilatancy relationships are proposed for each section of the stress path to evaluate the increments in volume change due to dilatancy.

(5) The simulations of stress paths and stress–strain relationships of Toyoura sand subjected to undrained cyclic torsional shear loadings were significantly improved after employing the proposed four-phased stress–dilatancy relationship.

(6) Complete liquefaction and steady state can be accurately simulated by the proposed model; however, further modifications are required to address the strain-softening behavior at large strain levels of dense sand.

In order to develop a generalized three-dimensional model based on the proposed stress–strain description, extended research has been initiated as preliminarily described by Namikawa et al. (2011) on the results from a numerical simulation of drained cyclic loading behavior. To maintain the objectivity, in terms of the independence from the coordinate systems, the three-dimensional model adopts the concept of an infinite number of nesting surfaces (Mroz et al., 1978). Its application to the simulation of undrained cyclic loading behavior, as is the case with the current study, is under way. Details will be reported elsewhere.

Acknowledgments

Our special appreciation goes to Prof. R. Uzuoka of the University of Tokushima, Japan, for his valuable suggestions in developing the cyclic elasto-plastic model. In addition, the authors sincerely acknowledge the Ministry of Education, Culture, Sports, Science, and Technology (Grants-in-Aid for Scientific Research #21360221), Japan for providing the financial assistance for the current research.

References

Balakrishnaiyer, K., Koseki, J., 2000. Modelling of stress–strain relationships of a reconstituted gravel subjected to large cyclic loading. In: Elnashai, A. S., Antoniou, S. (Eds.), Implications of Recent Earthquakes on Seismic Risk: Series on Innovation in Structures and Construction, vol. 2; 2000, pp. 105–114.

Chiaro, G., Kiyota, T., Koseki, J., 2013. Strain localization characteristics of loose saturated Toyoura sand in undrained cyclic torsional shear tests with initial static shear. Soils Found. 53 (1), 23–34.

Chiaro, G., Koseki, J., Sato, T., 2012. Effects of initial static shear on liquefaction and large deformation properties of loose saturated Toyoura sand in undrained cyclic torsional shear tests. Soils Found. 52 (3), 498–510.

De Silva, L.I.N., Koseki, J., 2012. Modelling of sand behavior in drained cyclic shear. In: Miura (Ed.), Advances in Transportation Geotechnics II. CRC Press, pp. 686–691.

De Silva, L.I.N., Koseki, J., Sato, T., 2006. Effects of different pluviation techniques on deformation property of hollow cylinder sand specimens. In: Proceedings of the International Symposium on Geomechanics and Geotechnics of Particulate Media, Ube, Yamaguchi, Japan, pp. 29–33.

De Silva, L.I.N., Koseki, J., Sato, T., Wang, L., 2005. High capacity hollow cylinder apparatus with local strain measurements. Proceedings of the Second Japan–U.S. Workshop on Testing, Modeling and Simulation, vol. 156. Geotechnical Special Publication, ASCE16–28.

De Silva, L.I.N., Koseki, J., Wahyudi, S., Sato, T., 2014. Stress–dilatancy relationships of sand in the simulation of volumetric behavior during cyclic torsional shear loadings. Soils Found. 54 (4), 845–858.

HongNam, N., Koseki, J., 2005. Quasi-elastic deformation properties of Toyoura sand in cyclic triaxial and torsional loadings. Soils Found. 45 (5), 19–38.

HongNam, N., Koseki, J., 2008. Deformation characteristics of dry Toyoura sand in large cyclic torsional loading and their modeling. In: Burns, Mayne, Santamarina (Eds.), Proceedings of the Fourth International Symposium on Deformation Characteristics of Geomaterials, vol. 2, IS Atlanta, USA, pp. 801–807.

Iai, S., Matsunaga, Y., Kameoka, T., 1992. Strain space plasticity model for cyclic mobility. Soils Found. 32 (2), 1–15.

Ishihara, K., Li, S., 1972. Liquefaction of saturated sand in triaxial torsion shear test. Soils Found. 12 (2), 19–39.

Ishihara, K., Tatsuoka, F., Yasuda, S., 1975. Undrained deformation and liquefaction of sand under cyclic stresses. Soils Found. 15 (1), 29–44.

Jefferie, M.G., 1993. Nor-Sand: a simple critical state model for sand. Géotechnique 43 (1), 91–103.

Kiyota, T., Sato, T., Koseki, J., Abadimarand, M., 2008. Behavior of liquefied sand under extremely large strain levels in cyclic torsional shear tests. Soils Found. 48 (5), 727–739.

Koseki, J., Hamaya, S., Tatsuoka, F., Maeshiro, N., 1998. Elastoplastic deformation characteristics of Toyoura sand during liquefaction. Geotechnical Engineering and Soil Dynamics III, vol. 75. Geotechnical Special Publication, ASCE385–397.

Koseki, J., Yoshida, T., Sato, T., 2005. Liquefaction properties of Toyoura sand in cyclic torsional shear tests under low confining stress. Soils Found. 45 (5), 103–113.

Ling, H.I., Yang, S., 2006. Unified sand model based on the critical state and generalized plasticity. J. Eng. Mech. 132 (12), 1380–1391.

Liou, C.P., Richart, F.E., Streeter, V.L., 1977. Numerical model for liquefaction. J. Geotech. Eng. Div. ASCE, 103; 589–606.

Liyanapathirana, D.S., Poulos, H.G., 2002. A numerical model for dynamic soil liquefaction analysis. Soil Dyn. Earthq. Eng. 22 (9–12), 1007–1015.

Masuda, T., Tatsuoka, F., Yamada, S., Sato, T., 1999. Stress-strain behavior of sand in plane strain compression, extension and cyclic loading tests. Soils Found. 39 (5), 31–45.

Mroz, Z., Norris, V.A., Zienkiewicz, O.C., 1978. An anisotropic hardening model for soils and its application to cyclic loading. Int. J. Numer. Anal. Methods Geomech. 2, 203–221.

Namikawa, T., Koseki, J., De Silva, L.I.N., 2011. Three dimensional modeling of stress-strain relationship of sand subject to large cyclic loading. In: Proceedings of the 5th International Conference on Earthquake Geotechnical Engineering. Santiago, Chile, paper-ID: TMSNA, CD-ROM, pp. 1–10.

Nishimura, S., 2002. Development of Three Dimensional Stress–Strain Model of Sand Undergoing Cyclic Undrained Loading and Stress–Axes Rotation (M.Eng. thesis). Dept. of Civil Engineering, The University of Tokyo, Japan.

Nishimura, S., Towhata, I., 2004. A three-dimensional stress–strain model of sand undergoing cyclic rotation of principal stress axes. Soils Found. 44 (2), 103–116.

Oka, F., Yashima, A., Kato, M., Sekiguchi, K., 1992. A constitutive model for sand based on the non-linear kinematic hardening rule and its application. In: Proceedings of 10th World Conference on Earthquake Engineering, pp. 2529–2534.

Oka, F., Yashima, A., Tateishi, Y., Taguchi, Y., Yamashita, S., 1999. A cyclic elasto-plastic constitutive model for sand considering a plastic-strain dependence of the shear modulus. Geotechnique 49 (5), 661–680.

Seed, H.B., Lee, K.L., 1966. Liquefaction of saturated sands during cyclic loading. Proc. ASCE SM6, 105–134.

Tatsuoka, F., Shibuya, S., 1991. Modelling of non-linear stress–train relations of soils and rocks – Part 2: new equation, Seisan-kenkyu. J. IIS Univ. Tokyo 43 (10), 435–437.

Tatsuoka, F., Jardine, R.J., Lo Presti, D., Di Benedetto, H., Kodaka, T., 1997. Characterising the pre-failure deformation properties of geomaterials, Theme Lecture for the Plenary Session No. 1, Proceedings of XIV IC on SMFE, vol. 4, Hamburg, pp. 2129–2164.

Tatsuoka, F., Masuda, T., Siddiquee, M.S.A., Koseki, J., 2003. Modeling the stress–strain relations of sand in cyclic plane strain loading. J. Geotech. Geoenviron. Eng. ASCE, 129; 450–467.

Towhata, I., Ishihara, K., 1985a. Shear work and pore water pressure in undrained shear. Soils Found. 25 (3), 73–85.

Towhata, I., Ishihara, K., 1985b. Undrained strength of sand undergoing cyclic rotation of principal stress axes. Soils Found. 25 (2), 135–147.

Vaid, Y., Thomas, J., 1995. Liquefaction and postliquefaction behavior of sand. J. Geotech. Eng. 121 (2), 163–173.